PCCP

PAPER

View Article Online
View Journal | View Issue

Cite this: *Phys. Chem. Chem. Phys.*, 2015, **17**, 7411

New *meso*-substituted corroles possessing pentafluorophenyl groups – synthesis and spectroscopic characterization†

Bartosz Bursa,[a] Bolesław Barszcz,[b] Waldemar Bednarski,[b] Jan Paweł Lewtak,[c] Dominik Koszelewski,[c] Olena Vakuliuk,[c] Daniel T. Gryko*[c] and Danuta Wróbel*[a]

Received 4th December 2014,
Accepted 30th January 2015

DOI: 10.1039/c4cp05648e

www.rsc.org/pccp

The investigation presented in this paper deals with new free-base corroles substituted with different peripheral groups. These aromatic macrocycles were efficiently synthesized by a [2+1] approach from dipyrromethanes. Moreover, the basic spectroscopic studies of the dyes in chloroform were conducted, and the UV-Vis absorption, fluorescence and ESR parameters were estimated. The experimental data were supported by quantum chemical calculations. The presence of monomeric dye structures is concentration independent (10^{-6}–10^{-4} M), as expected for dyes in a solvent of low polarity, and rules out aggregate formation of corroles dissolved in chloroform. The excitation emission and fluorescence life-time values confirm the monomeric structure of the corroles. The spectra were compared with the time-dependent density functional theory (TD-DFT) results for the HOMO–LUMO states. The ESR examinations strongly show that for any type of studied fluorine corrole an unpaired electron is localized on the corrole macroring but not on the substituents both before and after light illumination. Laser illumination creates additional radicals, however with different effectiveness depending on the sample.

1. Introduction

Corroles are synthetic aromatic porphyrin-analogue dyes, in which one *meso* carbon bridge is absent[1–8] which leads to the redistribution of electron density when one compares them to porphyrins[9] and in consequence this can result in changes of spectroscopic properties and make them promising candidates as photoactive agents. The similar but not the same molecular structure of corroles with respect to porphyrins, large delocalized π-electron conjugation, reasonable stability and very good matching of their absorption spectrum range to sunlight make them new excellent organic materials for light energy collection and conversion. Thus, in some laboratories corroles have attracted considerable interest because of their potential applications as photoconductors, in electronic devices, as gas sensors, solar cells and in other photo-electroactive items.[10–18]

Selected photophysical properties of some corroles have been previously studied by us with the use of various spectroscopic methods: UV-Vis spectroscopy, infrared absorption, Raman scattering and electron paramagnetic resonance.[19–21] Our experimental methods were supported by quantum chemical calculations. In this paper we wish to describe the synthesis and to present the spectroscopic characterization of six new *meso*-substituted corroles possessing various groups of different electronic and steric character. In particular corroles bearing naphthalene-1-yl substituents (and analogous ones) at position 10 were studied. Thus, the general purpose of the presented paper is to investigate the fundamental electronic properties by UV-vis spectroscopy (absorption, fluorescence, and electron spin resonance (ESR)) supported by quantum-chemical calculations. Gaining in-depth knowledge of the relationship between structure and optical properties is essential for potential applications of corroles in optoelectronics and related fields.

2. Materials and methods

2.1. Synthesis

2,7-Dimethoxynaphthalene, 4,7-dimethoxy-1-naphthaldehyde, 2,3-dichloro-5,6-dicyano-*p*-benzoquinone (DDQ), indium(III) chloride and pyrrole were purchased from Sigma-Aldrich. All chemicals were used as received unless otherwise noted. Reagent grade solvents (DCM, hexanes) were distilled prior to use. All reported ^{1}H NMR spectra were collected using a 400 or

[a] *Faculty of Technical Physics, Institute of Physics, Poznan University of Technology, 60-965 Poznań, Poland. E-mail: danuta.wrobel@put.poznan.pl*
[b] *Institute of Molecular Physics, Polish Academy of Sciences, 60-179 Poznań, Poland*
[c] *Institute of Organic Chemistry, Polish Academy of Sciences, 01-224 Warsaw, Poland. E-mail: daniel@icho.edu.pl*

† Electronic supplementary information (ESI) available. See DOI: 10.1039/c4cp05648e

500 MHz spectrometer. Chemical shifts (δ ppm) were determined with TMS as the internal reference; J values are given in Hz. The UV-Vis absorption spectra were recorded in THF. The absorption wavelengths are reported in nm. Flash column chromatography was performed on silica (200–400 mesh). The mass spectra were obtained by field desorption MS (FD-MS) and electrospray ionisation (ESI-MS). The following compounds have been prepared according to literature procedures: 2,7-dimethoxy-1-naphthalenecarbaldehyde,[22] 5-pentafluorophenyldipyrromethane,[23] 8-methoxy-4-quinolinecarboxaldehyde[24], 4-formyl-7,8-dimethoxycoumarin,[25] corrole **5**[26] and corrole **6**.[27]

10-(4,7-Dimethoxynaphthalen-1-yl)-5,15-bis(pentafluorophenyl)-corrole (1). 4,7-Dimethoxy-1-naphthaldehyde (108 mg, 0.5 mmol) and 5-pentafluorophenyldipyrromethane (312 mg, 1 mmol) were dissolved in MeOH (50 mL). Subsequently, a solution of HCl_{aq} (36%, 2.5 mL) in H_2O (50 mL) was added, and the reaction was stirred at room temperature for 1 h. The mixture was extracted with $CHCl_3$ (2 × 50 mL), and the organic layer was washed twice with H_2O, dried (Na_2SO_4), filtered, and diluted to 250 mL with $CHCl_3$. DDQ (300 mg, 1.3 mmol) was added, and the mixture was stirred for 0.5 h at room temperature. The reaction mixture was concentrated to half the volume and was passed through a silica column (silica, DCM/hexanes, 1 : 1). All fractions containing corrole were combined and evaporated to dryness. Flash column chromatography (silica, DCM/hexanes, 1 : 4) afforded the title compound as a dark solid. The resulting solid was precipitated from hot DCM by adding cyclohexane. The crystals were filtered off and dried under vacuum to give 115 mg of pure corrole **1** (28%). R_f (DCM/hexanes, 1 : 1) = 0.57; ^{1}H NMR (400 MHz, $CDCl_3$, Me_4Si, ppm) δ (−2.5)–(−1) (br s, 3H, NH), 2.94 (s, 3H, OCH_3), 4.24 (s, 3H, OCH_3), 6.47 (d, 1H, J = 2.3 Hz, naphtha.), 7.08 (d, 1H, J = 7.9 Hz, naphtha.), 7.15 (dd, 1H, J_1 = 2.5, J_2 = 9.3 Hz, naphtha.), 8.02 (d, 1H, J = 7.9 Hz, naphtha.), 8.46 (d, 1H, J = 9.3 Hz, naphtha.), 8.50 (d, 2H, J = 4.6 Hz, β-H), 8.56 (br s, 2H, β-H), 8.60 (d, 2H, J = 4.4 Hz, β-H), 9.10 (d, 2H, J = 4.0 Hz, β-H); HRMS (ESI): [MH^+] 817.1678 $C_{43}H_{23}F_{10}N_4O_2$ requires: 817.1655. Anal. calcd for $C_{43}H_{22}F_{10}N_4O_2$: C, 63.24; H, 2.72; N, 6.86. Found: 63.33; H, 2.70; N, 6.71.

10-(2,7-Dimethoxynaphthalen-1-yl)-5,15-bis(pentafluorophenyl)-corrole (2)

Method A. 2,7-Dimethoxy-1-naphthalenecarbaldehyde (108 mg, 0.5 mmol) and 5-pentafluorophenyldipyrromethane (312 mg, 1 mmol) were dissolved in MeOH (50 mL). Subsequently, a solution of HCl_{aq} (36%, 2.5 mL) in H_2O (50 mL) was added, and the reaction was stirred at room temperature for 1 h. The mixture was extracted with $CHCl_3$ (2 × 50 mL), and the organic layer was washed twice with H_2O, dried (Na_2SO_4), filtered, and diluted to 250 mL with $CHCl_3$. DDQ (300 mg, 1.3 mmol) was added, and the mixture was stirred overnight at room temperature. The reaction mixture was concentrated to half the volume and was passed through a column (silica, DCM/hexanes, 1 : 3). All fractions containing corrole were combined and evaporated to dryness. Flash column chromatography (silica, DCM/hexanes, 1 : 9 → 1 : 4) afforded the title compound as a dark solid. The resulting solid was suspended in hot MeOH, cooled, and filtered to give pure corrole **2** (19 mg, 4.7%).

Method B. 2,7-Dimethoxy-1-naphthalenecarbaldehyde (108 mg, 0.5 mmol) and 5-pentafluorophenyldipyrromethane (312 mg, 1 mmol) were dissolved in a pre-prepared solution of TFA (10 μL) in DCM (10 mL). After 1 h at room temperature the reaction mixture was dissolved in DCM (800 mL), a solution of DDQ (300 mg, 1.3 mmol) in toluene (3 mL) was added, and the reaction was stirred at room temperature for an additional 0.5 h. The reaction mixture was passed through a silica column (silica, DCM/hexanes, 1 : 3). All fractions containing corrole were combined and evaporated to dryness. Flash column chromatography (silica, DCM/hexanes, 1 : 9 → 1 : 4) afforded the title compound as a dark solid. The resulting solid was suspended in hot MeOH, cooled, and filtered to give pure corrole **2** (73 mg, 18%). R_f (DCM/hexanes, 1 : 1) = 0.60; ^{1}H NMR (400 MHz, $CDCl_3$, Me_4Si, ppm) δ (−3)–(−1) (br s, 3H, NH), 2.87 (s, 3H, OCH_3), 3.61 (s, 3H, OCH_3), 6.20 (d, 1H, J = 2.5 Hz, naphtha.), 7.03 (dd, 1H, J_1 = 2.5, J_2 = 9 Hz, naphtha.), 7.54 (d, 1H, J = 9.1 Hz, naphtha.), 7.94 (d, 1H, J = 9.1 Hz, naphtha.), 8.20 (d, 1H, J = 9.0 Hz, naphtha.), 8.41 (d, 2H, J = 4.6 Hz, β-H), 8.53 (d, 2H, J = 3.2 Hz, β-H), 8.58 (d, 2H, J = 4.8 Hz, β-H), 9.07 (d, 2H, J = 4.3 Hz, β-H); HRMS (FD): [M^+] 816.1606 $C_{43}H_{22}F_{10}N_4O_2$ requires: 816.1583. Anal. calcd for $C_{43}H_{22}F_{10}N_4O_2$: C, 63.24; H, 2.72; F, 23.26, N, 6.86. Found: 63.01; H, 2.78; F, 23.18, N, 6.97.

10-(8-Methoxyquinolin-4-yl)-5,15-bis(pentafluorophenyl)-corrole (3). 8-Methoxy-4-quinolinecarboxaldehyde (160 mg, 0.85 mmol) and 5-pentafluorophenyldipyrromethane (530 mg, 1.7 mmol) were dissolved in DCM (55 mL). To the resulting mixture TFA (200 μL) was added and the reaction mixture was stirred for 30 min. Subsequently Et_3N (400 μL) was added and, after diluting with DCM to 300 mL, a solution of DDQ (550 mg, 2.38 mmol) in toluene (10 mL) was added, and the reaction was stirred at room temperature for a further 0.5 h. The reaction mixture was passed through a silica pad (silica, DCM/acetone, 95 : 5). All fractions containing corrole were combined and evaporated to dryness. Flash column chromatography (silica, DCM/acetone, 95 : 5) afforded the title compound as a dark solid. The resulting solid was precipitated from hot DCM by adding hexanes. The crystals were filtered off and dried under vacuum to give 121 mg of corrole **3** (18%). R_f (DCM/MeOH 99 : 1) = 0.50; ^{1}H NMR (500 MHz, $CDCl_3$, Me_4Si, ppm) δ (−3)–(−1) (br s, 3H, NH), 3.00 (s, 3H, OCH_3), 6.52 (d, 1H, J = 2.8 Hz, quin.), 7.42 (dd, 1H, J_1 = 2.8, J_2 = 9.4 Hz, quin.), 8.04 (d, 1H, J = 4.2 Hz, quin.), 8.24 (d, 1H, J = 9.4Hz, quin.), 8.41 (d, 2H, J = 4.8 Hz, β-H), 8.59 (d, 2H, J = 4.1 Hz, β-H), 8.65 (d, 2H, J = 4.6 Hz, β-H), 9.07 (d, 1H, J = 4.2 Hz, quin.), 9.14 (d, 2H, J = 4.3 Hz, β-H); HRMS (TOF MS FD): [M^+]: 787.1457 $C_{41}H_{19}N_5OF_{10}$ requires: 787.1430. UV-vis (THF) λ 328, 412, 566, 609 nm.

10-(7,8-Dimethoxycoumarin-4-yl)-5,15-bis(pentafluorophenyl)-corrole (4). 4-Formyl-7,8-dimethoxycoumarin (47 mg, 0.20 mmol) and 5-pentafluorophenyldipyrromethane (125 mg, 0.4 mmol) were dissolved in a pre-prepared solution of TFA (20 μL) in DCM (10 mL). After 20 min at room temperature the reaction mixture was diluted with DCM (50 mL) and a solution of DDQ (118 mg, 0.52 mmol) in toluene (2 mL) was added, and the reaction was stirred at room temperature for an additional 0.5 h. The reaction mixture was passed through a silica pad (silica, DCM/acetone, 95 : 5). All fractions containing corrole

were combined and evaporated to dryness. Flash column chromatography (silica, DCM/acetone, 95 : 5) afforded the title compound as a dark solid. The resulting solid was precipitated from hot DCM by adding hexanes. The crystals were filtered off and dried under vacuum to give 121 mg of corrole **4** (16%). R_f (DCM/acetone 98 : 2) = 0.58; ^{1}H NMR (400 MHz, $CDCl_3$, Me_4Si, ppm) δ (−3)–(−2) (br s, 3H, NH), 3.83 (s, 3H, OCH_3), 4.20 (s, 3H, OCH_3), 6.49 (s, 2H, coumar.), 6.99 (s, 1H, coumar.), 8.57 (br s, 2H, β-H), 8.72–8.75 (m, 4H, β-H), 9.13 (br s, 2H, β-H); HRMS (TOF MS ESI): [MH^+]: 835.1397 $C_{42}H_{21}F_{10}N_4O_4$ requires: 835.1364; UV-vis (THF) λ 413, 422, 566, 607 nm.

2.2. Spectroscopic investigations

UV-Vis spectra of the samples **1–6** in chloroform (ε = 4.80) were recorded with the use of a Cary 4000 UV-Vis spectrometer in the range 300–800 nm, and fluorescence emission (λ_{exc} = 405 nm) and excitation spectra (λ_{em} = 700 nm) were recorded with the use of a Hitachi 4500 Fluorometer. Absorption and fluorescence spectra in solution were recorded for 10^{-4}, 10^{-5} and 10^{-6} M concentrations. Fluorescence kinetics were determined with the use of a PTI instrument. The values of the life-time were evaluated with the use of the Launch EasyLife V program.

Continuous wave X-band ESR experiments were carried out using a Bruker ELEXSYS 500 EPR spectrometer equipped with a Super High Sensitivity Probehead resonator and a helium gas-flow cryostat (ESR900, Oxford Instruments). Dark and light spectra were recorded at 250 K for a chloroform solution with a 10^{-5} M fluorine corrole concentration. Light spectra were recorded immediately after solution illumination (30 mW cm^{-2}, 1 min) which was performed directly in the resonator with 405 nm semiconductor laser light. The number of radicals was obtained after double integration of the EPR spectra and comparison with a DPPH standard. The concentration of free radicals was calculated in relation to the number of corrole molecules.

2.3. Computational details

In order to interpret the experimental UV-Vis spectra we performed calculations of the transition energies by means of time-dependent density functional theory (TD-DFT). The calculations were performed using the B3LYP hybrid functional (Becke 3-parameter exchange functional combined with Lee–Yang–Parr correlational functional) and the standard 6-31G basis set. The choice of the functional was made taking into account the results published in ref. 28, in which a few functionals were applied to the TD-DFT calculations of corroles. It was concluded that to reproduce the energetic relations between the electronic transitions, the use of hybrid functionals like B3LYP is most reasonable. The calculations were run on the equilibrium geometries of isolated molecules obtained from the optimization procedure performed earlier for all the investigated corroles (DFT, B3LYP/6-31G).[45] The Gaussian 03 program package was used for that purpose.[29] The first 200 transitions have been calculated. To convolute the resulting transition energies and oscillator strengths into the absorption spectra the GaussSum program was used.[30] The spectra were generated assuming a FWHM (full width at half maximum) parameter equal to 3000 cm^{-1} for all transitions.

2.4. Photophysical parameters

Fluorescence quantum yield (Φ_F) is determined by the comparative method according to eqn (1)[31,32]

$$\Phi_F = \Phi_{Ref}\frac{F \cdot A_{Ref} \cdot n^2}{F_{Ref} \cdot A \cdot n_{Ref}^2} \quad (1)$$

where F and F_{Ref} are the areas under the fluorescence emission curves of samples **1–6** and the references, respectively; A and A_{Ref} are the relative absorbance of the sample and the references at the excitation wavelength; n and n_{Ref} are the refractive indices of the solvents and the references. As a reference chlorophyll *a* in methanol was used (Φ_{Ref} = 0.32[33]). The samples and the reference were excited at the same wavelength (405 nm).

3. Results and discussion

3.1. Design and synthesis

Six carefully designed corroles were synthesized for this study. *meso*-substituted *trans*-A_2B-corroles possessing two pentafluorophenyl substituents at positions 5 and 15 were chosen as a key motif due to their stability[12,27] which is crucial in advanced photophysical studies. Structural diversity has been achieved by attaching substituents differing in steric and electronic effects at position 10. We selected the following substituents: 4-nitrophenyl (strongly electron-withdrawing, lack of steric hindrance), 2,7-dimethoxynaphthalen-1-yl and 4,7-dimethoxynaphthalen-1-yl (electron-donating, steric hindrance), 4-methoxyquinoliny-1-yl (basic nitrogen atom, steric hindrance) and 5,6-dimethoxycoumarin-1-yl (strongly polarized, steric hindrance). 5,10,15-Tris(pentafluorophenyl)corrole (**5**) has also been studied as a reference point. The synthesis of all the *trans*-A_2B-corroles was performed according to the well-known [2+1] condensation of dipyrromethanes[34] with aldehydes under either classical TFA–DCM[27] or in the H_2O–MeOH–HCl system[35] (Scheme 1). The corresponding aldehydes were prepared following literature procedures.[22,24,25] Interestingly the yield of corroles **1–4** depends both on the conditions and on the electronic character of the aldehyde. In the case of 4,7-dimethoxynaphthaldehyde, the condensation in polar solvents afforded corrole **1** in high yield (Scheme 1). On the other hand, the analogous reaction involving 2,7-dimethoxynaphthaldehyde led to the corresponding corrole **2** in 5% yield only. This can be partly rationalized based on the lipophilic character of that aldehyde, which is not compatible with the H_2O–MeOH–HCl system. The same reaction performed in CH_2Cl_2 afforded corrole **2** in 18% yield. The same conditions were also used for formyl-coumarin to give corrole **4** in 16% yield. *meso*-substituted corroles, bearing a coumarin moiety attached to a corrole core by various linkers have been prepared before.[37,38] It is worth noting that the yield of corrole **4** was significantly higher than the efficiency of the condensation of 5-pentafluorophenyldipyrromenthane with other formyl-coumarins leading to previously described coumarin-corroles (~5–8%).[37,38] This can be rationalized by the much weaker polarization of 4-formyl-7,8-dimethoxycoumarin compared

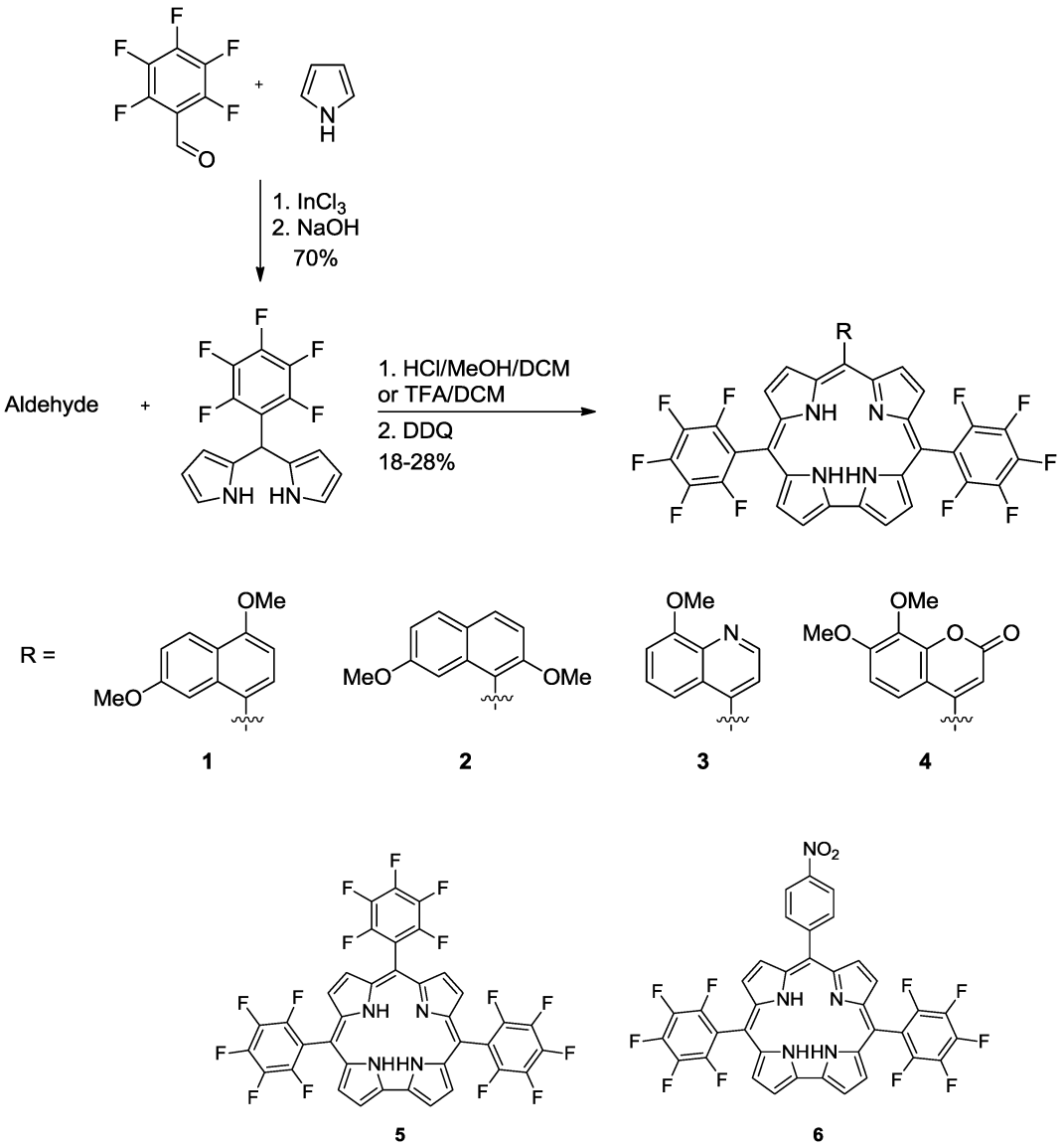

Scheme 1 Synthesis and molecular structures of the investigated corroles.

to previously employed formyl-coumarins, which leads to a lower number of side-reactions. For the condensation of 4-formyl-8-methoxyquinoline, the conditions previously optimized for aldehydes bearing basic nitrogen atoms were utilized,[36] giving corrole **3** in 18% yield (Scheme 1). Corroles **5** and **6** were prepared following known procedures.[26,27]

3.2. Electronic absorption spectra

Experimental. The electronic absorption spectra of corroles **1–6** in chloroform at three concentrations (10^{-6}, 10^{-5} and 10^{-4} M) have been measured. In Fig. 1 we present representative spectra of the corroles **1** and **5**. The spectra are normalized to unity at the highest Soret band. The second derivative spectra of **1** and **5** are also shown as an example. For the remaining dyes one does not observe any influence of concentration on the spectra shape, as expected for dyes in solvent of low polarity. The spectra of the dyes are slightly different in their shapes. Similarities of the shapes of samples **2** and **6** to that of sample **1**, and the shapes of samples **3** and **4** to that of sample **5**, are shown. The location of the bands and the full widths at half maximum (FWHM) are almost independent of the dye concentration; this indicates the presence (or high predominance) of monomeric dye structures in the whole range of dye concentrations. This conclusion is in agreement with Ziegler *et al.*;[39] they ruled out the presence of aggregates in corroles dissolved in non-polar chloroform.

The two-structural band in the Soret region with maxima at 410 and 427 nm indicates the presence of at least two electronic transitions. Also the band in Fig. 1 observed at 562 nm is broad and split into two bands at 556 and 573 nm. Additionally, the long wavelength band (638 nm) is also present. Table 1A gathers the band intensity ratios as well as the values of the FWHM (of the dyes at a concentration of 10^{-6} M).

The previously described coumarin-corroles[37,38] usually contained either π-expanded coumarins or strongly polarized

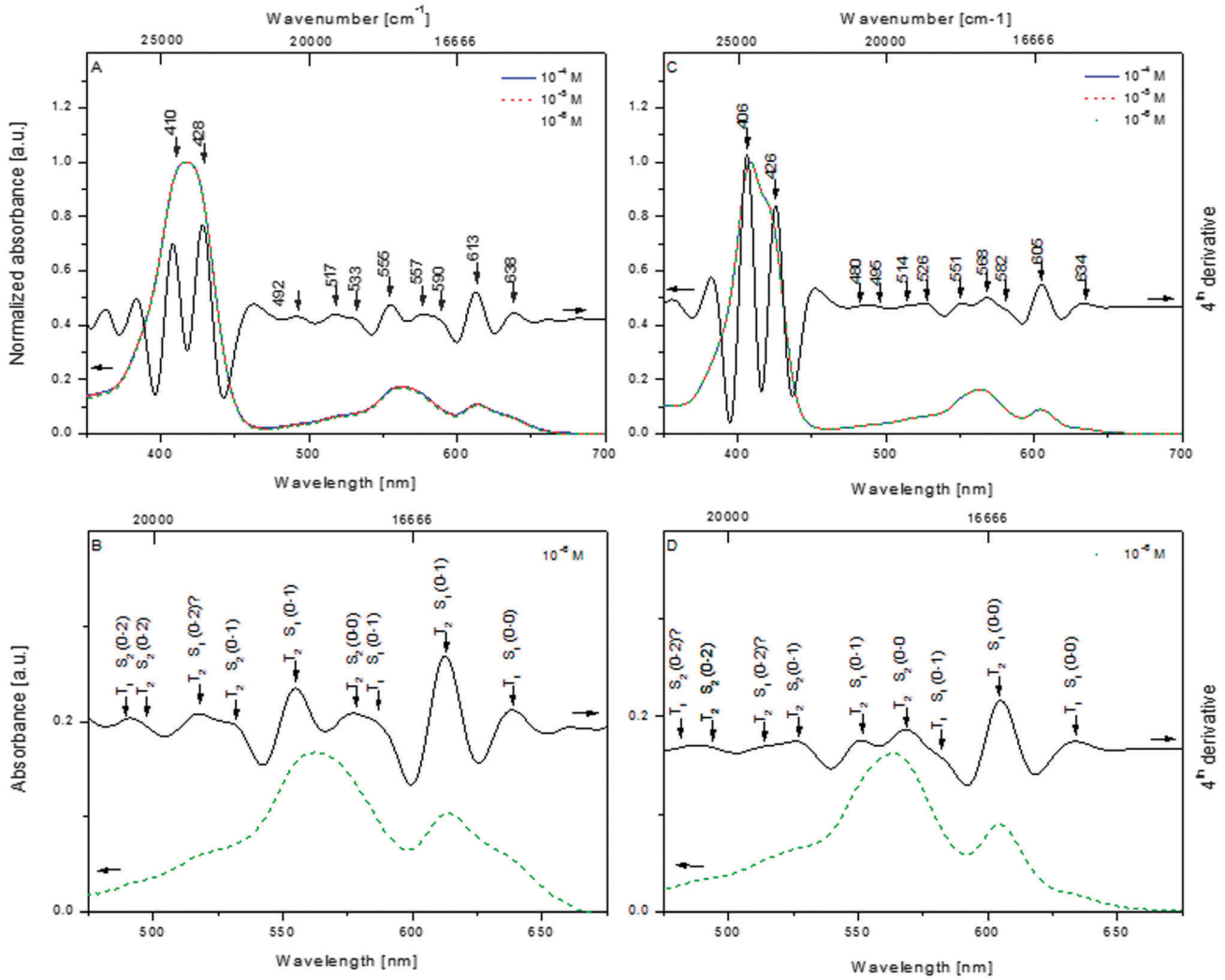

Fig. 1 Representative absorption spectra and derivative spectra of corroles **1** (A, B) and **5** (C, D) in chloroform; concentration 10^{-4}–10^{-6} M; normalized to unity at the highest Soret band. The remaining dyes show concentration independence. B and D show the range 450–700 nm with notation of the transition assignments.

coumarins bearing an electron-donating group at position 7. In spite of these differences both the absorption and emission spectra of corrole **4** (Fig. 5–7) bear a strong resemblance to previous dyads with a very visible shoulder on the Soret band and two distinct Q-bands (560–570 nm and 610–620 nm).

The origin of the absorption bands is discussed on the basis of Gouterman's four orbital model[40] and our TD-DFT calculations presented in this paper. The corroles are much less symmetric (their symmetry is C_{2v}) whereas porphyrins are characterized by D_{2h} or D_{4h} symmetry.[41,42] Nevertheless, the four-orbital model refers also to corrole systems.[43,44] The reduced symmetry strongly affects the absorption properties.[43,44] The absorption bands of corroles contain intense Soret bands and weaker Q bands. In our absorption experiments two sets of bands are well recognized, in the region of 400–450 nm and of 500–700 nm. In the decomposition of the Soret and Q bands it is useful to analyze the spectra and assign the bands of the tautomer electronic transitions as proposed by Beenken *et al.*[28] Two different types of tautomers of the studied corroles are expected and can be identified – they are denoted as T1 and T2 (Table 1B). Five of them belong to the A_2B-type corroles (two *meso*-positions are occupied with different groups – samples **1**–**4** and **6**) and one corrole is the A_3-type (*meso*-positions are substituted with the same groups – sample **5**). We conducted our absorption experiments at room temperature, thus it should be expected that a thermodynamic equilibrium with a balance of the two tautomers T1 and T2 in coexistence would be obtained. The results of the experimental data, supported by means of the derivative absorption Gaussian analysis and by the Gouterman model of the electronic transitions of the two tautomers T1 and T2, are gathered in Table 1B. The four-orbital model predicts the presence of four electronic transitions. On the basis of Table 1B the following electronic transitions can be identified as belonging to the tautomers T1 and T2. The $S_1(0–0)$ transitions can be assigned to T1 and T2 in the ranges of 635–638 nm and 605–613 nm, respectively. The $S_2(0–0)$ transitions are observed in the range of 568–577 nm. Some overtones $S_1(0–1)$, $S_2(0–1)$ and $S_2(0–2)$ are also identified. At this point of our discussion it is worth noting that in one of our papers[45] we have also presented

Table 1 (A) Selected absorption and fluorescence parameters; the data of the absorption maxima were evaluated on the basis of the Gaussian decomposition.[a] (B) Band analysis of the absorption spectra of the studied corroles at room temperature by means of fourth derivative minima, and the band assignment to the transitions of the tautomers T1 and T2 in the Q-band range by means of the Gouterman model[b 40]

(A)

Dye	Φ_F	Band intensity ratio		Absorption maximum [nm]				FHWM [cm^{-1}]				R^2	τ [ns]	χ^2
1	0.31	410/427	1.05	374	394	410	427	722	750	580	636	0.9990	3.96 ± 0.09	1.51
2	0.30	407/423	0.98	371	391	407	423	626	766	522	700	0.9977	4.27 ± 0.11	0.95
3	0.27	408/425	1.12	380	392	408	425	477	477	580	617	0.9894	4.30 ± 0.14	1.45
4	0.25	410/425	1.15	380	390	410	425	667	534	486	644	0.9955	4.37 ± 0.15	1.27
5	0.21	407/424	1.22	379	392	407	424	637	475	545	568	0.9925	4.95 ± 0.41	1.38
6	0.07	407/427	1.06	374	390	407	427	755	562	723	1045	0.9932	1.26 ± 0.09	0.86

(B)

Dye	Corrole type	Experimental maximum position		Gouterman model	Assignment	
		nm	cm^{-1}		T1	T2
1	A_2B	638	15 674	15 740	$S_1(0–0)$	
		613	16 313	16 695		$S_1(0–0)$
		590	16 949	17 040	$S_1(0–1)$	
		577	17 331	17 570		$S_2(0–0)$
		555	18 018	17 995		$S_1(0–1)$
		548		**18 250**	**$S_2(0–0)$**	
		545		**18 340**	**$S_1(0–2)$?**	
		533	18 762	18 870		$S_2(0–1)$
		517	19 342	19 295		$S_1(0–2)$?
		510	19 608	19 550	$S_2(0–1)$	
		492	20 325	20 170		$S_2(0–2)$
		480	20 833	20 850	$S_2(0–2)$?	
2	A_2B	638	15 674	15 740	$S_1(0–0)$	
		612	16 340	16 695		$S_1(0–0)$
		588	17 007	17 040	$S_1(0–1)$	
		575	17 391	17 570		$S_2(0–0)$
		554	18 051	17 995		$S_1(0–1)$
		548		**18 250**	**$S_2(0–0)$**	
		545		**18 340**	**$S_1(0–2)$?**	
		530	18 868	18 870		$S_2(0–1)$
		518	19 305	19 295		$S_1(0–2)$?
		512	19 531	19 550	$S_2(0–1)$	
		495	20 202	20 170		$S_2(0–2)$
		483	20 704	20 850	$S_2(0–2)$?	
3	A_2B	638	15 674	15 740	$S_1(0–0)$	
		609	16 420	16 695		$S_1(0–0)$
		583	17 153	17 040	$S_1(0–1)$	
		573	17 545	17 570		$S_2(0–0)$
		553	18 083	17 995		$S_1(0–1)$
		548		**18 250**	**$S_2(0–0)$**	
		545		**18 340**	**$S_1(0–2)$?**	
		529	18 904	18 870		$S_2(0–1)$
		514	19 455	19 295		$S_1(0–2)$?
		507	19 724	19 550	$S_2(0–1)$	
		491	20 367	20 170		$S_2(0–2)$
		478	20 921	20 850	$S_2(0–2)$?	
4	A_2B	636	15 724	15 740	$S_1(0–0)$	
		608	16 447	16 695		$S_1(0–0)$
		583	17 153	17 040	**$S_1(0–1)$**	
		571	17 513	17 570		$S_2(0–0)$
		553	18 083	17 995		$S_1(0–1)$
		548		**18 250**	**$S_2(0–0)$**	
		545		**18 340**	**$S_1(0–2)$?**	
		528	18 939	18 870		$S_2(0–1)$
		515	19 417	19 295		$S_1(0–2)$?
		509	19 646	19 550	$S_2(0–1)$	
		492	20 325	20 170		$S_2(0–2)$
		483	20 704	20 850	$S_2(0–2)$?	
5	A_3	634	15 773	15 740	$S_1(0–0)$	
		605	16 529	16 695		$S_1(0–0)$

Table 1 (*continued*)

(B)

Dye	Corrole type	Experimental maximum position		Gouterman model	Assignment	
		nm	cm^{-1}		T1	T2
		582	17 182	17 040	$S_1(0–1)$	
		568	17 606	17 570		$S_2(0–0)$
		551	18 149	17 995		$S_1(0–1)$
		548		**18 250**	**$S_2(0–0)$**	
		545		**18 340**	**$S_1(0–2)$?**	
		526	19 011	18 870		$S_2(0–1)$
		514	19 455	19 295		$S_1(0–2)$?
		508	19 685	19 550	$S_2(0–1)$	
		495	20 202	20 170		$S_2(0–2)$
		480	20 833	20 850	$S_2(0–2)$?	
6	A_2B	640	15 625	15 740	$S_1(0–0)$	
		610	16 393	16 695		$S_1(0–0)$
		587	17 036	17 040	$S_1(0–1)$	
		573	17 452	17 570		$S_2(0–0)$
		555	18 018	17 995		$S_1(0–1)$
		548		**18 250**	**$S_2(0–0)$**	
		545		**18 340**	**$S_1(0–2)$?**	
		531	18 832	18 870		$S_2(0–1)$
		517	19 342	19 295		$S_1(0–2)$?
		510	19 608	19 550	**$S_2(0–1)$**	
		496	20 161	20 170		$S_2(0–2)$
		480	20 833	20 850	**$S_2(0–2)$?**	

[a] FWHM – full width at half maximum (calculated with the Gaussian component program), R^2 – coefficient of determination, Φ_F – fluorescence quantum yield, τ – fluorescence life-time, χ^2 – chi square. [b] Bands expected by the model but not found in the analysis of the experimental spectrum are given in bold. Questionable assignments are marked by "?", precision ± 0.5 nm.

the results of some vibrational bands and also the combination bands with the use of very sensitive infrared photoacoustic examinations. However, a few bands predicted in the Gouterman model are not seen (*e.g.* $S_1(0–2)$ and $S_2(0–0)$).

Quantum chemical calculations. Our supposition as to the spectral behavior of the corrole dyes was confirmed by quantum-chemical calculations. The electronic transitions (oscillator strengths *versus* wavelength) calculated by the TD-DFT method for all investigated corroles are presented in Fig. 2. In all cases the Soret band (about 400 nm) consists of 3–4 intense transitions. However, the spectral distance between the transitions is quite small and they appear in the resulting spectra as single bands. In the experimental spectra the Soret band is observed also as a single band (with some components visible), so there is an

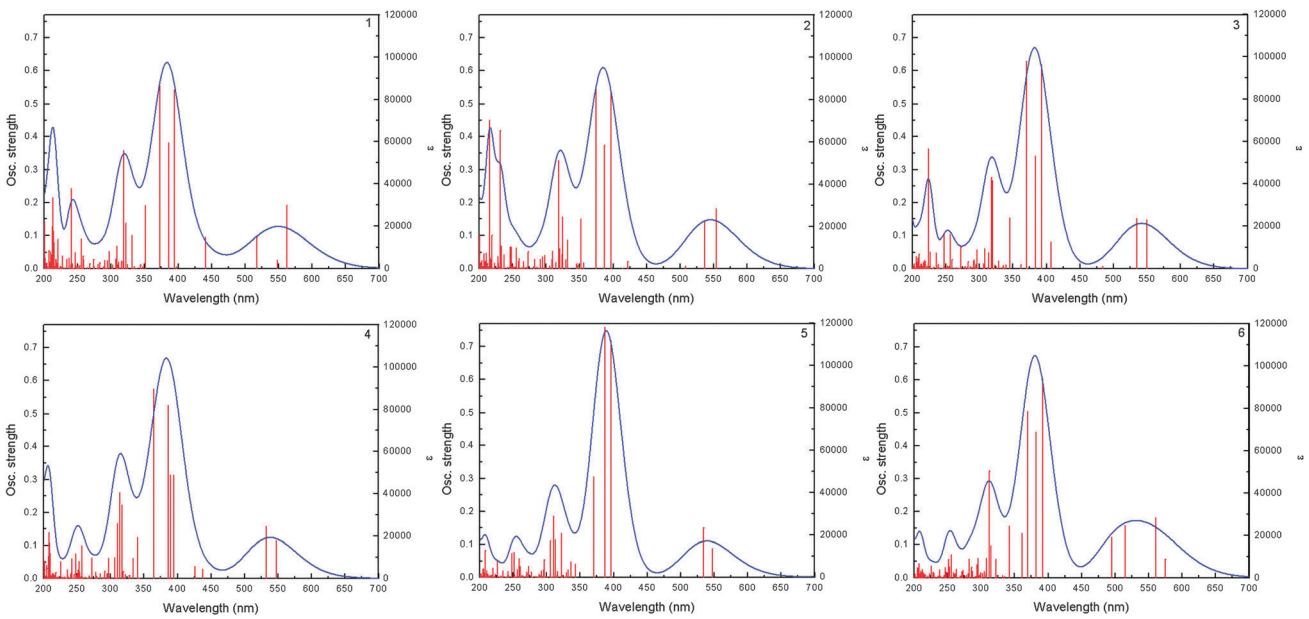

Fig. 2 Electronic transitions (oscillator strengths *versus* wavelength) calculated by the TD-DFT method for all the investigated corroles.

agreement between the calculated and experimental spectra. In the Q band spectral region, two bands are observed in all the experimental spectra (614 and 638 nm). In the calculated spectra, the band is not separated but can be seen in Fig. 2; there are two (or more) intense transitions in this region. A similar result has been obtained in calculations done by Salvatori *et al.*[46] for a set of free-base and copper corroles. The electronic transition related to the appearance of the Q band involves mainly the HOMO (highest occupied molecular orbital) and LUMO (lowest unoccupied molecular orbital). Of course other orbitals also take part but the dominant contribution arises from the HOMO → LUMO transition. The main transitions with appropriate descriptions are collected in Table 3. The HOMO and LUMO energies and the HOMO–LUMO energy gap values calculated for the investigated corroles are collected in Table 2 and Fig. 3 while the contour plots of the mentioned orbitals are gathered in Fig. 4.

Table 2 HOMO and LUMO energies and the HOMO–LUMO energy gap values calculated for the investigated corroles (eV). The values calculated for similar free base corroles by Salvatori and Beenken are provided for comparison

	1	2	3	4	5	6	Ref. 46	Ref. 28
E_{total} (hartree)	−3018.805	−3018.802	−2920.335	−3129.867	−3132.251	−2840.650		
HOMO	−5.20	−5.14	−5.39	−5.58	−5.63	−5.58	−4.76	−5.244
LUMO	−2.75	−2.69	−2.91	−3.05	−3.10	−3.16	−2.30	−2.595
Δ_{H-L}	2.45	2.45	2.48	2.53	2.53	2.42	2.46	2.649

Table 3 Selected electronic transitions calculated for the investigated corroles using the TD-DFT (B3LYP/6-31G) method. The major contributions of the involved orbitals are also given. The table is limited to the transitions with wavelength > 350 nm and oscillator strengths > 0.1

Wavelength (nm)	Oscillator strength	Major contribution
1		
562.1	0.1918	H − 2 → LUMO (15%), HOMO → LUMO (63%)
394.3	0.5418	H − 1 → L + 1 (13%), HOMO → L + 1 (26%)
385.5	0.3818	H − 4 → LUMO (40%), H − 2 → L + 1 (16%), H − 1 → L + 1 (12%)
372.4	0.554	H − 4 → LUMO (45%), H − 1 → L + 1 (17%)
351.1	0.1907	HOMO → L + 2 (68%)
2		
553.5	0.1816	H − 1 → LUMO (22%), H − 1 → L + 1 (14%), HOMO → LUMO (43%), HOMO → L + 1 (15%)
536.4	0.1418	H − 1 → LUMO (40%), HOMO → LUMO (24%), HOMO → L + 1 (21%)
396.8	0.5368	H − 1 → LUMO (14%), HOMO → L + 1 (38%)
387.0	0.3744	H − 4 → LUMO (42%), H − 1 → L + 1 (23%)
374.1	0.5476	H − 4 → LUMO (45%), H − 1 → L + 1 (23%)
351.6	0.1501	HOMO → L + 2 (56%), HOMO → L + 3 (14%)
3		
549.3	0.1476	H − 1 → LUMO (28%), H − 1 → L + 1 (12%), HOMO → LUMO (36%), HOMO → L + 1 (19%)
534.6	0.1521	H − 1 → LUMO (34%), H − 1 → L + 1 (10%), HOMO → LUMO (30%), HOMO → L + 1 (19%)
392.3	0.6197	H − 1 → LUMO (14%), HOMO → L + 1 (35%)
383.1	0.3415	H − 4 → LUMO (42%), H − 2 → L + 1 (13%), H − 1 → L + 1 (14%)
370.0	0.6289	H − 4 → LUMO (39%), H − 1 → L + 1 (21%)
4		
547.2	0.1142	H − 1 → LUMO (32%), H − 1 → L + 1 (11%), HOMO → LUMO (31%), HOMO → L + 1 (22%)
531.9	0.1582	H − 1 → LUMO (28%), H − 1 → L + 1 (13%), HOMO → LUMO (35%), HOMO → L + 1 (17%)
394.1	0.3133	H − 1 → L + 1 (26%), H − 1 → L + 2 (30%)
389.2	0.3133	H − 1 → L + 2 (47%), HOMO → L + 1 (15%)
385.9	0.5257	H − 2 → L + 1 (15%), H − 1 → L + 1 (14%), H − 1 → L + 2 (14%), HOMO → L + 1 (16%)
364.3	0.5745	H − 4 → LUMO (18%), H − 2 → L + 1 (41%), H − 1 → L + 1 (13%)
5		
534.2	0.1511	H − 1 → LUMO (21%), H − 1 → L + 1 (16%), HOMO → LUMO (40%), HOMO → L + 1 (15%)
395.7	0.7181	H − 1 → LUMO (18%), HOMO → L + 1 (33%)
386.8	0.7593	H − 2 → LUMO (16%), H − 1 → L + 1 (37%)
369.7	0.3045	H − 2 → LUMO (74%), H − 1 → L + 1 (10%)
6		
560.3	0.1808	H − 1 → LUMO (19%), H − 1 → L + 2 (10%), HOMO → LUMO (46%)
514.6	0.1576	H − 1 → LUMO (22%), H − 1 → L + 1 (14%), HOMO → L + 1 (24%), HOMO → L + 2 (33%)
494.7	0.1214	H − 1 → LUMO (13%), H − 1 → L + 1 (60%), H − 1 → L + 2 (11%)
391.3	0.6029	H − 1 → LUMO (12%), HOMO → L + 2 (38%)
381.8	0.4419	H − 2 → LUMO (32%), H − 2 → L + 1 (11%), H − 1 → L + 2 (29%)
368.9	0.505	H − 2 → LUMO (55%), H − 1 → L + 2 (22%)
360.8	0.1345	H − 2 → L + 1 (76%)

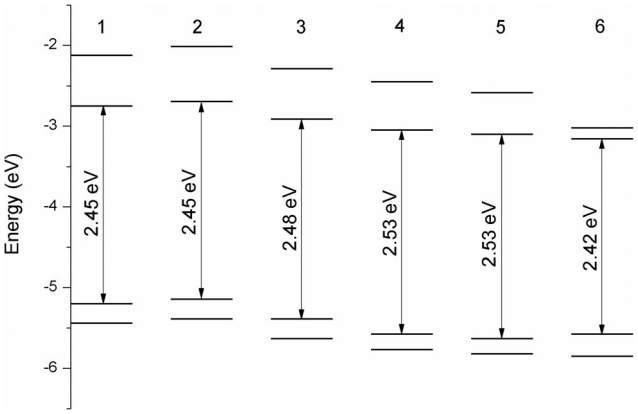

Fig. 3 HOMO–LUMO energy gap values calculated for the investigated corroles.

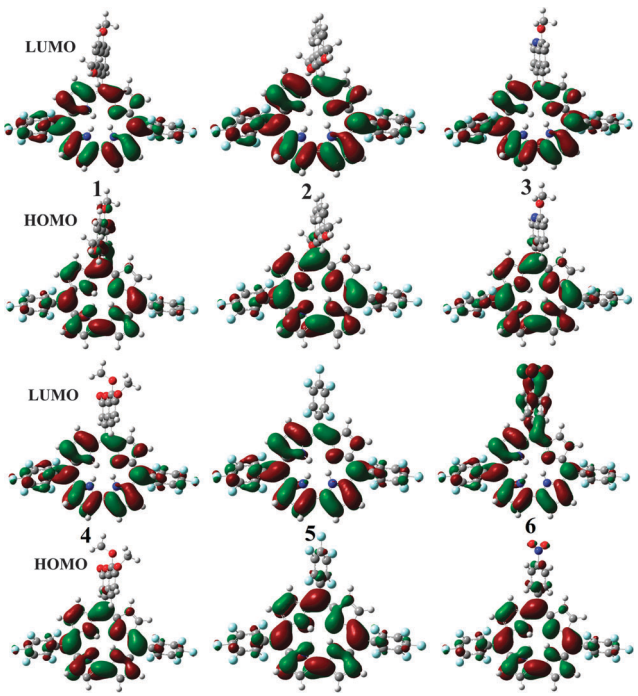

Fig. 4 Contour plots of the corrole molecular orbitals.

It is easy to notice some differences in the HOMO and LUMO energy values. The greatest differences are between the HOMO levels of **5** and **2** (0.49 eV) and the LUMO levels of **6** and **2** (0.47 eV). Despite that, the energy gap between the HOMO and LUMO is very similar for all the investigated corroles – the greatest difference is between that of **6** and those of **4**/**5** (0.11 eV). The energy gap and the HOMO–LUMO energy values are also similar to the ones calculated by Salvatori[46] and Beenken[28] for similar free-base corroles (see Table 2 for comparison).

In the investigated molecules both the HOMO and the LUMO are localized on the corrole ring and not on the substituents. The only exception is the LUMO of **6** which is localized on the corrole macroring and on one of the substituents. The reason for this is the presence of the electron-withdrawing nitro group in the substituent. Selected electronic transitions calculated for the investigated corroles using the TD-DFT (B3LYP/6-31G) method are shown in Table 3. The major contributions of the involved orbitals are also given. The table is limited to the transitions with wavelengths > 350 nm and oscillator strengths > 0.1.

3.3. Fluorescence studies

The studied corroles exhibit strong fluorescence; Fig. 5 shows the results for all the dyes in chloroform when excited at 405 nm. The character of the fluorescence spectra is typical for the porphyrin-like corroles. As seen, the spectra are dependent on the samples and differ from each other in shapes and location of the maxima. The bands of samples **1** and **6** are located at about 651 nm and the bands of **2–5** at about 642 nm; weak bands in the range 700–750 nm are also seen. Moreover, the fluorescence of the samples is characterized by small humps observed in the shorter wavelength range (600–625 nm), which are very well seen in the spectra of samples **2–6** and much less in that of sample **1**. The differences in the shapes of the fluorescence spectra can be compared with our TD-DFT results and the tautomer T1 and T2 absorption band analysis by means of the Gouterman model. Thus, the predominant fluorescence is seen in the long wavelength region and can be assigned to the emission of the tautomer T1; the less intense shorter wavelength humps can have their origin in the fluorescence of T2.[28,47] The differences in the sample fluorescence behavior come from the presence of the various substituents attached to the main corrole core. Similar fluorescence behavior was shown by Kruk *et al.*[13] for other NH *meso*-(dichloropyrimidinyl)corrole tautomers, although the T2 tautomer emission in their work was much more intense than that of our samples.

The higher intensity of T2 seems to be influenced strongly by the electron-withdrawing character of the substituents at position 10. Both C_6F_5 (corrole **5**) and pyranone (corrole **4**) are electron-deficient. The same holds true for the nitro group (corrole **6**), but the nitro group quenches emission so its effect on the T1/T2 ratio is more complex.

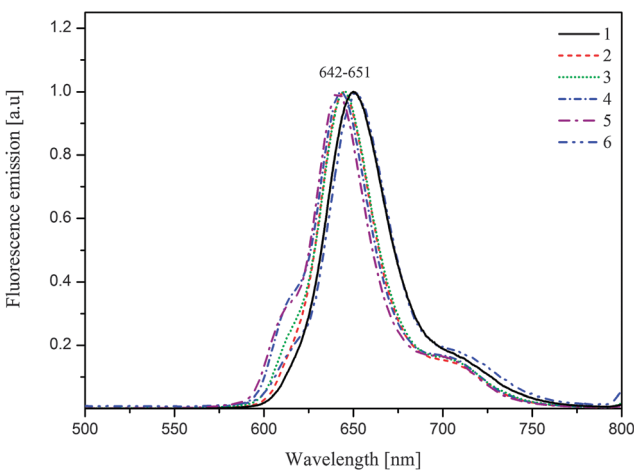

Fig. 5 Fluorescence spectra of the dyes in chloroform; excitation at 405 nm.

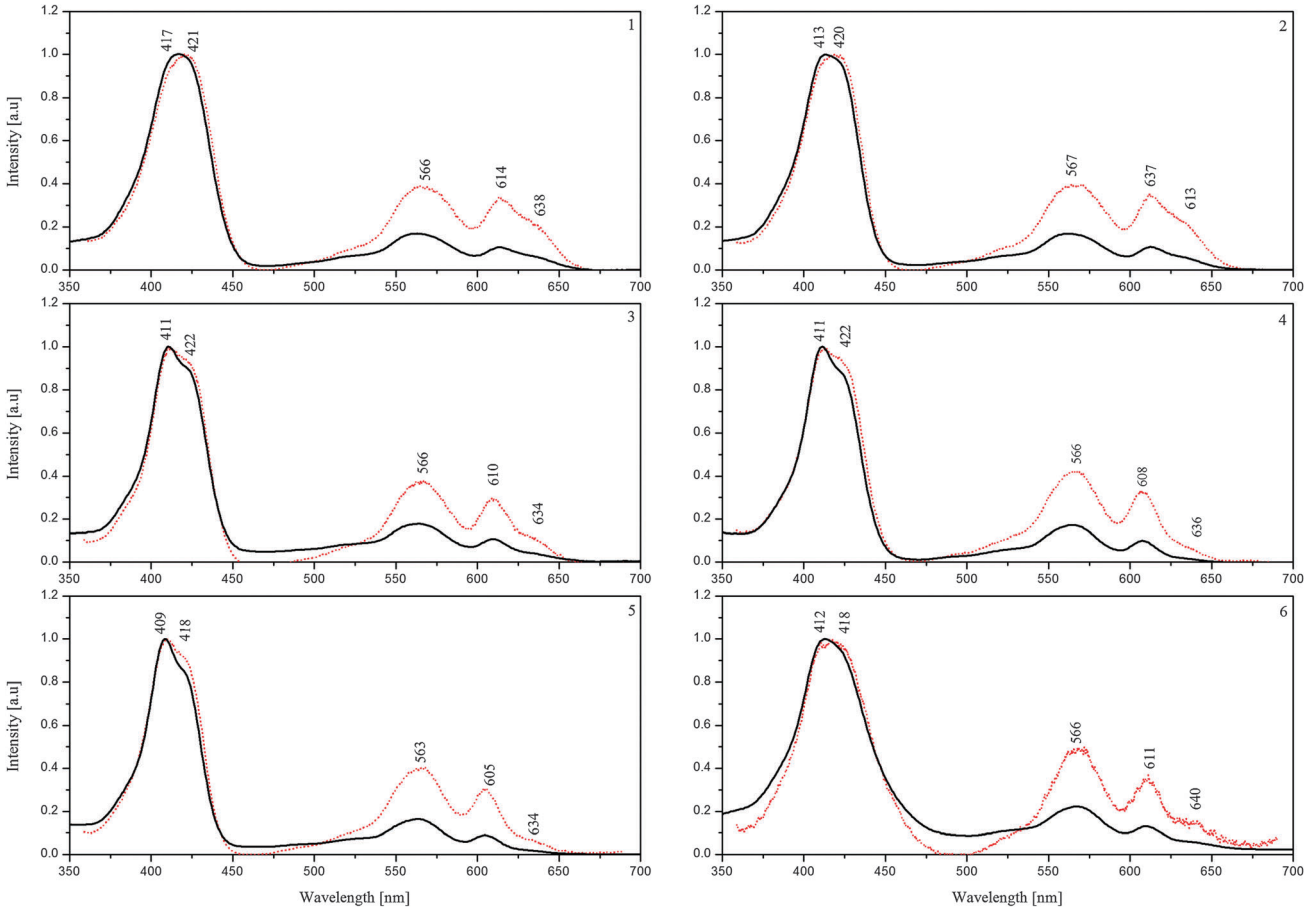

Fig. 6 Excitation emission spectra of the corroles observed at 700 nm.

The shapes of the excitation emission spectra observed at 700 nm correspond to those of the absorption spectra in the range 350–680 nm (Fig. 6). However, the exception is the slightly split band in the Soret region, which confirms the presence of the T1 and T2 tautomers.

The fluorescence decays of two selected dyes (1 and 6) in chloroform are shown in Fig. 7. On the basis of the fluorescence kinetics the life-time values are evaluated and the results are shown in Table 1A. The life-time values of 1.26–4.95 ns (depending on the dye) are characteristic of porphyrin-like dyes and confirm monomeric corrole emission. The results of the deconvolution procedure give the typical monoexponential decay; however we are not able to recognize the life-times of tautomers T1 and T2 in our experiment. In Table 1A the values of the fluorescence quantum yields are also collected.

3.4. ESR spectroscopy

Fig. 8 presents the qualitative changes in the ESR spectra recorded for samples **1–6** before and after illumination. Each fluorine corrole solution shows an almost symmetrical ESR line characterized by the parameters: line width ΔB_{pp} = 6.5 (± 0.1) Gs, *g*-factor g = 2.0030 (± 0.0002). The lack of differences in the ESR parameter values strongly suggests that for any of the studied fluorine corroles, an unpaired electron is localized on the corrole macroring but not on the substituents. The only noticeable difference among the samples is the ESR line amplitude, which is proportional to the number of radicals created. Because after illumination the shape of the ESR spectrum does not change and one can observe only increased line amplitude in comparison to the dark samples, we conclude that light creates some additional radicals of the same type as those of the samples before illumination.

Fig. 9 presents an example of ESR signal deconvolution for the light-induced sample **2**. Approximations indicate that any spectrum consists of two Gaussian lines. These two lines are characterized by different line widths, ΔB_{pp}^{1st} = 6 Gs and ΔB_{pp}^{2nd} = 8 Gs, and *g*-factors, g^{1st} = 2.0030 and g^{2nd} = 2.0032. The two components of the ESR spectrum result from the partial charge separation in the fluorine corrole molecules and the creation of cationic and anionic radicals.

The increase in the number of radicals (proportional to the ESR signal amplitude) under laser illumination and the decrease after the discontinuation of illumination due to partial ionic radical recombination can be described by the exponential function, with characteristic times of growth and decay of the order of a few minutes and a few hours, respectively. The concentrations of radicals in the solutions of the different fluorine corroles before and after 1 minute of illumination are presented in Fig. 10. It is worth mentioning that the ESR results also show radicals in the powdered samples, but their

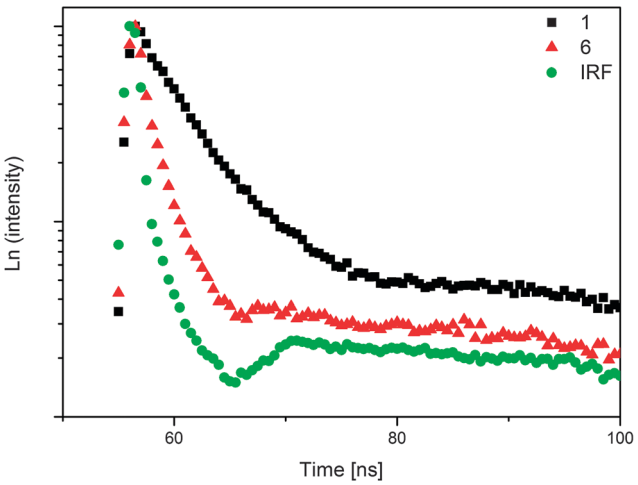

Fig. 7 Fluorescence kinetics of corroles **1** and **6** in chloroform.

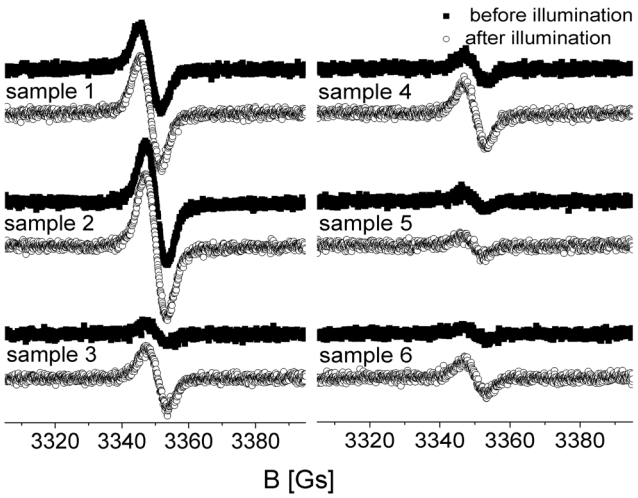

Fig. 8 ESR spectra of corroles **1–6** in chloroform (10^{-5} M), recorded at 250 K before and after laser illumination.

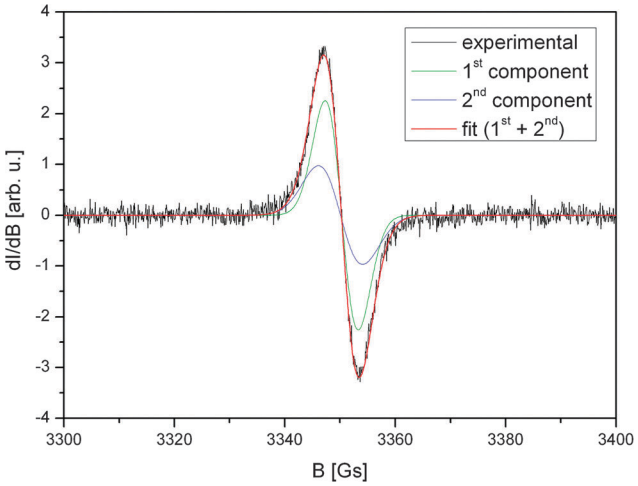

Fig. 9 Experimental and approximated ESR spectra of the light-induced sample **2**.

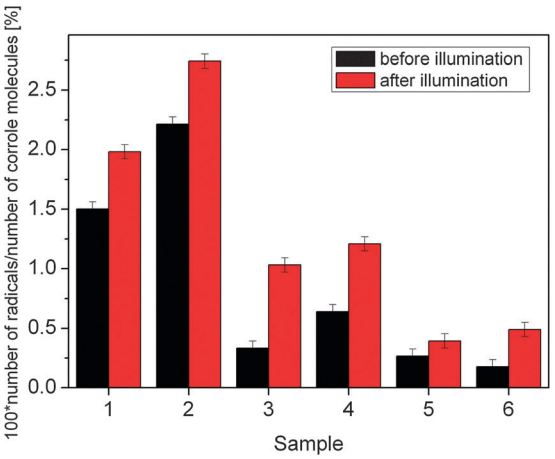

Fig. 10 Concentrations of radicals in corrole solutions before and after laser illumination: 30 mW cm^{-2}, 1 min, 405 nm.

concentration is much smaller and does not exceed 0.02% (at least about one order of magnitude less in comparison to those in solution). The creation of radicals most probably results from an activation process. In the case of solution samples the activation energy of radical creation is lowered and leads to an increase of radical concentration. As presented in Fig. 10, samples **1** and **2** show the highest concentrations of radicals (above 1.50%) before laser illumination. Samples **5** and **6** have the lowest concentrations under the same conditions, *i.e.* 0.27% and 0.18%, respectively. One minute of laser illumination creates additional radicals in all of the samples. This process is most effective in sample **3** (0.70% additional radicals) and the least efficient in sample **5** (0.13%).

4. Conclusions

In summary we can conclude the following:

(1) The free-base corroles possessing partly polarized structures due to the presence of two strongly electron-withdrawing C_6F_5 groups, in chloroform show a monomeric structure even in solutions of high concentrations. This is confirmed by the absorption and excitation emission as well as the fluorescence experiments (intensity ratio, FWHM parameters and fluorescence life-time). The multi-structural character of the bands in the Soret and in the Q-band regions (410–427 nm, 500–650 nm) indicate the presence of more than one electronic transition assigned to the tautomers T1 and T2. The emission spectra evidently show the predominance of the T1 tautomer fluorescence in the room temperature spectra.

(2) The experimental data are supported by quantum chemical calculations (TD-DFT) of the HOMO and LUMO, and the agreement between the experimental and simulated results is evident. In the investigated molecules (samples **1–5**) both the HOMO and the LUMO are localized on the corrole ring and not on the substituents. The only exception is the LUMO of **6**which is localized on the corrole macroring and on the nitro substituent.

(3) The ESR experiments strongly show that an unpaired electron is localized on the corrole macroring but not on the substituents both before and after light illumination – laser illumination creates additional radicals, however with different effectiveness depending on the sample.

Abbreviations

UV-vis	Ultraviolet–visible
ESR	Electron spin resonance
FWHM	Full width at half maximum
TD-DFT	Time-dependent density functional theory

Acknowledgements

The paper was supported by the Poznan University of Technology (grant 06/62/DSPB/0215; B.B1, B.B2, D.W.) and by EuroSolarFuels grant.

References

1 D. T. Gryko, J. P. Fox and D. P. Goldberg, *J. Porphyrins Phthalocyanines*, 2004, **8**, 1091.
2 C. J. Lemon and P. J. Brothers, *J. Porphyrins Phthalocyanines*, 2011, **15**, 809.
3 R. Paolesse, in *The Porphyrin Handbook*, ed. K. M. Kadish, K. M. Smith and R. Guilard, Academic Press, New-York, 2000, vol. 2, p. 201.
4 F.-P. Montforts, M. Glasenapp-Breiling and D. Kusch, in *Houben-Weyl Methods of Organic Chemistry*, ed. E. Schaumann, Thieme, Stuttgart-New York, 1998, vol. E9d, p. 665.
5 D. T. Gryko, *Eur. J. Org. Chem.*, 2002, 1735.
6 R. Guilard, J.-M. Barbe, C. Stern and K. M. Kadish, in *The Porphyrin Handbook*, ed. K. M. Kadish, K. M. Smith and R. Guilard, Elsevier, 2003, vol. 18, p. 303.
7 D. T. Gryko, J. P. Fox and D. P. Goldberg, *J. Porphyrins Phthalocyanines*, 2004, **8**, 1091.
8 S. Nardis, D. Monti and R. Paolesse, *Mini-Rev. Org. Chem.*, 2005, **2**, 355.
9 D. Wróbel and A. Graja, *Coord. Chem. Rev.*, 2011, **255**, 2555.
10 I. Aviv and Z. Gross, *Chem. Commun.*, 2007, 1987 and references therein.
11 L. You, H. Shen, L. Shi, G. Zhang, H. Li, H. Wang and L. Ji, *Sci. China: Phys., Mech. Astron.*, 2010, **53**, 1491.
12 L. Flamigni and D. T. Gryko, *Chem. Soc. Rev.*, 2009, **38**, 1635.
13 M. Kruk, T. H. Ngo, P. Verstappen, A. Starukhin, J. Hofkens, W. Dehaen and W. Maes, *J. Phys. Chem. A*, 2012, **116**, 10695.
14 M. Kruk, T. H. Ngo, V. Savva, A. Starukhin, W. Dehaen and W. Maes, *J. Phys. Chem. A*, 2012, **116**, 10704.
15 Y. B. Ivanova, V. Savva, N. Z. Marmardashvili, A. Starukhin, T. H. Ngo, W. Dehaen, W. Maes and M. Kruk, *J. Phys. Chem. A*, 2012, **116**, 10683.
16 J. M. Barbe, G. Canard, S. Brandés and R. Guilard, *Eur. J. Org. Chem.*, 2005, 4601.
17 J. M. Barbe, G. Canard, S. Brandés and R. Guilard, *Angew. Chem., Int. Ed.*, 2005, **117**, 3163.
18 S.-L. Lai, L. Wang, C. Yang, M.-Y. Chan, X. Guan, C.-C. Kwok and C.-M. Che, *Adv. Funct. Mater.*, 2014, **24**, 4655.
19 K. Lewandowska, B. Barszcz, J. Wolak, A. Graja, M. Grzybowski and D. T. Gryko, *Dyes Pigm.*, 2013, **96**, 249.
20 K. Lewandowska, B. Barszcz, A. Graja, B. Bursa, A. Biadasz, D. Wróbel, W. Bednarski, S. Waplak, M. Grzybowski and D. T. Gryko, *Synth. Met.*, 2013, **166**, 70.
21 B. Bursa, D. Wróbel, K. Lewandowska, A. Graja, M. Grzybowski and D. T. Gryko, *Synth. Met.*, 2013, **176**, 18–25.
22 T. Mizutani, T. Murakami, T. Kurahashi and H. Ogoshi, *J. Org. Chem.*, 1996, **61**, 539.
23 A. Osuka, G. Noya, S. Taniguchi, T. Okada, Y. Nishimura, I. Yamazaki and N. Mataga, *Chem. – Eur. J.*, 2000, **6**, 33.
24 J.-P. Liou, C.-Y. Nien, C.-Y. Chang, J.-Y. Chang, Y.-C. Chen, C.-C. Kuo, H.-P. Hsieh, J.-S. Wu, S.-Y. Wu and J.-Y. Chang, *J. Med. Chem.*, 2010, **53**, 2309.
25 K. Bohra, B. Kumar, V. S. Parmar, A. K. Prasad, D. Sharma and C. E. Olsen, *J. Indian Chem. Soc.*, 2013, **90**, 1885.
26 D. T. Gryko and B. Koszarna, *Org. Biomol. Chem.*, 2003, **1**, 350.
27 D. T. Gryko and B. Koszarna, *Synthesis*, 2004, 2205.
28 W. Beenken, M. Presselt, T. H. Ngo, W. Dehaen, W. Maes and M. Kruk, *J. Phys. Chem. A*, 2014, **118**, 862.
29 M. J. Frisch, G. W. Trucks, H. B. Schlegel, G. E. Scuseria, M. A. Robb, J. R. Cheeseman, J. A. Montgomery, Jr., T. Vreven, K. N. Kudin, J. C. Burant, J. M. Millam, S. S. Iyengar, J. Tomasi, V. Barone, B. Mennucci, M. Cossi, G. Scalmani, N. Rega, G. A. Petersson, H. Nakatsuji, M. Hada, M. Ehara, K. Toyota, R. Fukuda, J. Hasegawa, M. Ishida, T. Nakajima, Y. Honda, O. Kitao, H. Nakai, M. Klene, X. Li, J. E. Knox, H. P. Hratchian, J. B. Cross, C. Adamo, J. Jaramillo, R. Gomperts, R. E. Stratmann, O. Yazyev, A. J. Austin, R. Cammi, C. Pomelli, J. W. Ochterski, P. Y. Ayala, K. Morokuma, G. A. Voth, P. Salvador, J. J. Dannenberg, V. G. Zakrzewski, S. Dapprich, A. D. Daniels, M. C. Strain, O. Farkas, D. K. Malick, A. D. Rabuck, K. Raghavachari, J. B. Foresman, J. V. Ortiz, Q. Cui, A. G. Baboul, S. Clifford, J. Cioslowski, B. B. Stefanov, G. Liu, A. Liashenko, P. Piskorz, I. Komaromi, R. L. Martin, D. J. Fox, T. Keith, M. A. Al-Laham, C. Y. Peng, A. Nanayakkara, M. Challacombe, P. M. W. Gill, B. Johnson, W. Chen, M. W. Wong, C. Gonzalez and J. A. Pople, *Gaussian 03, Revision D.01*, Gaussian, Inc., Pittsburgh, PA, 2003.
30 N. M. O'Boyle, A. L. Tenderholt and K. M. Langner, *J. Comput. Chem.*, 2008, **29**, 839.
31 J. Lakowicz, *Principles of Fluorescence Spectroscopy*, Springer, New York, 3rd edn, 2006.
32 M. A. M. J. Van Zandvoort, D. Wróbel, A. J. Scholten, D. De Jager, G. Ginkel and Y. K. Levine, *Photochem. Photobiol.*, 1993, **58**, 600.
33 H. Scheer, *Chlorophylls*, CRC-Press, Boca Raton, 1991.
34 D. T. Gryko, D. Gryko and C.-H. Lee, *Chem. Soc. Rev.*, 2012, **41**, 3780.

35 B. Koszarna and D. T. Gryko, *J. Org. Chem.*, 2006, **71**, 3707.
36 D. T. Gryko and K. E. Piechota, *J. Porphyrins Phthalocyanines*, 2002, **6**, 81.
37 M. Tasior, D. T. Gryko, D. J. Pielacińska, A. Zanelli and L. Flamigni, *Chem. – Asian J.*, 2010, **5**, 130–140.
38 M. Tasior, R. Voloshchuk, Y. M. Poronik, T. Rowicki and D. T. Gryko, *J. Porphyrins Phthalocyanines*, 2011, **15**, 1011–1023.
39 C. J. Ziegler, J. R. Sabin, G. R. Geiger III and V. N. Nemykin, *Chem. Commun.*, 2012, **48**, 4743.
40 M. Gouterman, G. H. Wagnière and L. C. Snyder, *J. Mol. Spectrosc.*, 1963, **11**, 108.
41 A. Biadasz, B. Bursa, B. Barszcz, A. Bogucki, B. Laskowska, A. Graja and D. Wróbel, *Dyes Pigm.*, 2011, **89**, 86.
42 D. Wróbel, A. Siejak and P. Siejak, *Sol. Energy Mater. Sol. Cells*, 2010, **94**, 492.
43 N. S. Hush, J. M. Dyke, M. L. Williams and I. S. Woolsey, *J. Chem. Soc., Dalton Trans.*, 1974, 395.
44 A. Ghosh, T. Wondimagegn and A. B. J. Parusel, *J. Am. Chem. Soc.*, 2000, **122**, 5100.
45 B. Barszcz, D. Wróbel, A. M. Urbańska, J. P. Lewtak, D. Koszelewski, O. Vakuliuk and D. T. Gryko, *Dyes Pigm.*, under review.
46 P. Salvatori, A. Amat, M. Pastore, G. Vitillaro, K. Sudhakar, L. Giribabu, Y. Soujanya and F. De Angelis, *Comput. Theor. Chem.*, 2014, **1030**, 59.
47 R. S. Becker, *Theory and Interpretation of Fluorescence and Phosphorescence*, Wiley Interscience, New York, 1969.